JOURNAL OF SOLID STATE CHEMISTRY **134,** 253–264 (1997)
ARTICLE NO. SC977551

Electrical Resistivity, Thermopower, and ^{57}Fe Mössbauer Study of $FeNbO_4$

E. Schmidbauer[1]

Institut für Allgemeine und Angewandte Geophysik der Universität München, Theresienstr. 41, 80333 Munich, Germany

and

J. Schneider

Institut für Kristallographie und Mineralogie der Universität München, Theresienstr. 41, 80333 Munich, Germany

Received December 30, 1996; in revised form July 15, 1997; accepted July 15, 1997

The electrical charge transport was investigated on sintered semiconducting $FeNbO_4$ and compositions with a slight surplus of Nb in the monoclinic (pseudorhombic) wolframite and orthorhombic α-PbO_2 structures using electrical DC, AC resistivity (complex plane impedance analysis), and thermopower Θ in the temperature T range ≈ 100–900 K. At low T, the experimental crystallite conductivity σ is consistent with a variable-range hopping charge transport model, characterized by the relationship $\ln \sigma \propto T^{-1/4}$. In the high-$T$ region, activation energies E_A for the extrapolated crystallite DC resistivity are found up to $E_A \approx 0.7$ eV. The thermopower Θ is negative, with $|\Theta|$ increasing with rising T in the low-T region, and between ≈ 120 and 300 K the data can be approximately described by a linear Θ–$T^{1/2}$ relation for both structures that is theoretically predicted for variable-range hopping. Above 300 K, the curves bend and Θ becomes constant with values Θ ∼ −270 and −220 to −230 μV/K. Suggesting electron hopping $Fe^{2+} \rightarrow Fe^{3-}$ to be the dominating charge transport mechanism, the Θ high-T data are in part compatible with the assumption that all or a dominant fraction of Fe^{2+} and Fe^{3+} are taking part in this process; this result follows from the derived concentration ratio $[Fe^{2+}]/[Fe^{3+}]$, which is similar to that determined from ^{57}Fe Mössbauer spectra at 79 K.

INTRODUCTION

Electrical properties of $FeNbO_4$ have been measured because of its possible use as an anode in photoelectrochemistry for solar energy conversion (1). $FeNbO_4$ is an end member of the mixed crystal series $Fe^{3+}Nb^{5+}O_4$ to $Fe^{2+}Nb_2^{5+}O_6$ ($Fe_{1-x/3}Nb_{1+x/3}O_4$, $0 \le x \le 1$) whose members occur in part as minerals (2–4). $FeNbO_4$ crystallizes in four modifications: (1) In the temperature range $T <$ 1080°C, it has the monoclinic (pseudorhombic) wolframite structure (space group $P2/c$); (2) in the region $1080 \le T \le$ 1380°C, it exhibits the orthorhombic α-PbO_2 structure (*Pbcn*); (3) for $T >$ 1380°C up to the melting point (≈ 1450°C), the tetragonal rutile structure ($P4_2/mnm$) has been observed (4–7); (4) a further monoclinic $FeNbO_4$ structure ($C2$) could be obtained by the gas transport preparation method in the temperature range 600–900°C (8).

In the wolframite lattice, there are zigzag chains of edge-sharing NbO_6 and FeO_6 octahedra along the [001] direction, with ordering of Fe and Nb. Each chain accommodates either Fe or Nb. Also in the α-PbO_2 structure, zigzag chains occur along [001] ; however, Fe and Nb are randomly distributed (Fig. 1). In the rutile structure, edge-sharing octahedra form straight chains along [001] with randomly arranged Fe and Nb.

The electrical conductivity σ of polycrystalline $FeNbO_4$ in the wolframite structure was found to be σ (294 K) ≈ $2.5 \times 10^{-5}\,\Omega^{-1}\,cm^{-1}$; $\ln \sigma$ vs $1/T$ was nonlinear at lower T (9). For polycrystalline $FeNbO_4$ in the α-PbO_2 structure, σ (294 K) ≈ $2.5 \times 10^{-2}\,\Omega^{-1}\,cm^{-1}$; the presence of a small concentration of Fe^{2+} was suggested to be the origin for the comparatively high σ (1). There is a difference of 3 orders of magnitude between the values.

We have investigated the electrical conduction in $FeNbO_4$, using DC and AC methods at various T. Impedance spectroscopy was applied, which was thought to enable distinction between different conduction processes. In addition, the thermopower was determined as a function of T. ^{57}Fe Mössbauer spectroscopy was utilized to detect possibly mixed valencies Fe^{2+} and Fe^{3+}. To elucidate the role of Fe^{2+} and Fe^{3+} for conduction in $FeNbO_4$, we increased slightly the Nb concentration (at the expense of Fe), which should lead to an enhanced Fe^{2+} content.

[1] To whom correspondence should be addressed.

0022-4596/97 $25.00

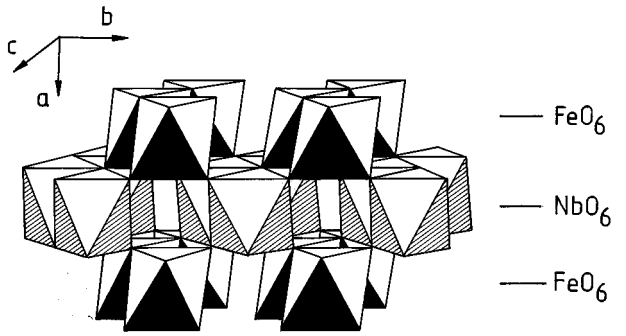

FIG. 1. Schematic view of the wolframite structure of $FeNbO_4$. FeO_6 and NbO_6 octahedra are ordered and are randomly distributed in the α-PbO_2 structure.

SAMPLE SYNTHESIS AND EXPERIMENTAL

Samples were prepared following the ceramic method starting from adequately mixed α-Fe_2O_3 (99.995%) and Nb_2O_5 (99.998%) powders. Small cylinders were pressed (2 kbar) and heated at 1100°C for 25 h in different gas atmospheres: (1) O_2 (1 atm), (2) air, (3) a $N_2/O_2 = 30$ (1 atm) gas mixture. After crushing, regrinding, and re-pressing, the products were treated at 1300°C for 50 h in the same atmospheres; this process was repeated. After the procedure, the furnace was switched off and the products were cooled at a rate of ≈ 300°C/h to 21°C in the mentioned gas atmospheres. It turned out that $FeNbO_4$, treated in this way, exhibits the wolframite structure. To ensure that materials with full wolframite or α-PbO_2 structures were obtained, samples used for electrical measurements were subjected to the following final treatment: (1) wolframite structure, prolonged heating at 1000°C for 8 days; (2) α-PbO_2 structure, heating at 1300°C for 50 h and quenching to ambient T within 5–6 min.

The sample composition was varied slightly. Three different compositions were prepared: $x = 0$, 0.02, and 0.05. The last two compositions were studied since a different Fe^{2+} concentration was expected relative to the dominating Fe^{3+} content. For $x = 0.02$ and 0.05, the same heating procedures were applied as described for $FeNbO_4$.

Cell constants were determined by X-ray analysis. An X-ray refinement analysis of diffractometer data with the Rietveld technique was made for all samples (Philips diffractometer, graphite monochromator, Cu$K\alpha$ radiation, and in part also a Stoe diffractometer, Mo$K\alpha$ radiation). Structural data for $FeNbO_4$ are quoted in Table 1; data of other workers are listed for comparison. In no case could any impurity phase be detected by X-rays.

For ^{57}Fe Mössbauer analysis, a conventional spectrometer with a sinusoidal drive was used (12 μC ^{57}Co/Rh).

TABLE 1
Fit Parameters of X-ray Diffractograms for $FeNbO_4$ in the Wolframite and α-PbO_2 Structures (Fig. 1)

	Wolframite ($P2/c$)		
Parameter	Cu($K\alpha1 + K\alpha2$)	Mo($K\alpha1$)	Ref. 10
R_{wp}/R_{exp}	1.53	0.99	1.48
R_{Bragg} (%)	8.7	8.0	
Fe^{3+}(2*f*): *y*	0.6742(8)	0.670(1)	0.6687
Nb^{5+}(2*e*): *y*	0.1807(5)	0.1825(3)	0.1824
O(1)(4*g*): *x*	0.940(2)	0.925(3)	0.919
O(1)(4*g*): *y*	0.138(2)	0.108(2)	0.116
O(1)(4*g*): *z*	0.774(2)	0.768(2)	0.767
O(2): *x*	0.425(2)	0.405(4)	0.418
O(2): *y*	0.384(2)	0.390(4)	0.384
O(2): *z*	0.725(2)	0.735(3)	0.738
a (Å)	4.6560(3)	4.6466(5)	4.637
b (Å)	5.6319(3)	5.6143(5)	5.607
c (Å)	5.0076(2)	4.9924(5)	4.992
β (deg)	90.27(7)	90.24(1)	90.06

	α-PbO_2 (*Pbcn*)	
Parameter	Cu($K\alpha1 + K\alpha2$)	Neutrons (11)
R_{wp}/R_{exp}	1.93	1.48
R_{Bragg} (%)	9.84	
Fe/Nb(4*c*) : *y*	0.1762(3)	0.1747(2)
O(8*d*): *x*	0.274(1)	0.2710(4)
O(8*d*): *y*	0.384(1)	0.3850(2)
O(8*d*): *z*	0.069(1)	0.0817(3)
a (Å)	4.6616(2)	4.6496(1)
b (Å)	5.6329(2)	5.618(1)
c (Å)	5.0164(2)	5.0058(1)

Absorber densities were ≈ 5 mg/cm^2. All isomer shift data are given relative to metallic Fe.

Sample examination under a light microscope revealed dense products (porosity < 0.05) with crystallite sizes of 50–100 μm. There was in some instances a tiny amount of a second phase ($< 0.5\%$) (below detection by X-rays); the same observation had been made earlier for $FeNbO_4$ (1). Sample preparation in O_2 did not lead to a different result. We found that a $N_2/O_2 = 30$ gas atmosphere during preparation led to an increased impurity phase of $\approx 1.5\%$. It appears that the formation of completely homogeneous $FeNbO_4$ may be possible for preparation in O_2 under high pressure. For $x = 0.05$ prepared in air, a homogeneous product without any impurity phase was detected.

DC and AC resistivities were determined in the range $80 \leq T \leq \approx 900$ K. For AC measurements, an LCR meter (HP4284A) was available that allowed data to be recorded in the frequency range 20 Hz to 1 MHz. Impedance spectroscopy was applied, plotting the real part of the impedance

versus the imaginary one in the complex impedance plane in order to be able to distinguish between different conduction processes. For polycrystalline metal oxides, the AC behavior can frequently be modeled by two equivalent circuits in series, each circuit being composed of an ohmic resistance R in parallel with a capacitor C, which are due to bulk and grain boundary processes (R_b, C_b and R_{gr}, C_{gr}). For bulk conductivity, typical capacity values are in the low pF/cm region whereas for grain boundary effects, larger capacities have been frequently observed (12–15).

Samples in the shape of parallelepipeds were cut from pellets with a wire saw. Afterward, the sample surfaces were carefully polished. Sample contacts were made with platinum paste (Leitplatin Demetron 308A), painted on opposite faces of a sample. After drying, the samples were heated at 450°C for 1 h to remove the binder and to obtain a densification of Pt grains. The samples were spring loaded between Pt plate electrodes. For AC measurements, a two-terminal method was used ($T < 300$ K) (sample dimensions $\approx 5 \times 2 \times 2$ mm^3); DC results for $T > 300$ K were obtained with a four-terminal configuration with four probes painted on two opposite faces (sample dimensions $\approx 7 \times 1.5 \times 1$ mm^3).

For thermopower Θ measurements, temperature gradients ΔT up to $\Delta T = 10$–15 K were generated across opposite contact faces of a sample using a microfurnace close to an electrode. Five different ΔT values were used and, for a fixed average T, the slope of the thermovoltage ΔU versus ΔT was used to determine $\Theta = \Delta U/\Delta T$. The measurements were carried out fully automatically using a PC program. At low T, Cu-cylinder electrodes and Cu leads were applied, and at high T, Pt-cylinder electrodes and Pt leads were used. Absolute Θ values are given, correcting the measured Θ for Θ_{Cu} or Θ_{Pt} according to $\Theta_{abs} = \Theta_{meas} + \Theta_{Pt/Cu}$ (16, 17). The thermovoltage ΔU was measured with a HP 3440H digital voltmeter (input resistance $> 10^{10}\,\Omega$). For calibration, stoichiometric polycrystalline Fe_3O_4 was used; the Θ results between 130 and 240 K were in good agreement with single-crystal data given in refs. 18 and 19, and in the high-T range up to ≈ 800 K with those presented in ref 20.

^{57}Fe MÖSSBAUER ANALYSIS

1. $FeNbO_4$ ($x = 0$)

Mössbauer spectra for samples $x = 0$, prepared in air or O_2, at 294 K differed for the wolframite and α-PbO_2 structures (Fig. 2). Doublets were recorded with different line widths in both cases. The spectrum for the wolframite structure could be adequately fit to a symmetrical quadrupole doublet; however, a similar fit for samples with the α-PbO_2 structure was unsatisfactory. The fit was notably improved by applying a second doublet (goodness of fit χ^2 from 5.2 to 1.4). Mössbauer parameters are listed in Table 2. The Fe^{3+} parameters resemble those known from other oxide materials. The spectrum of the α-PbO_2 structure can, hence, be described by two groups of Fe^{3+} which show different values of quadrupole splitting (QS). This result is related to a variation of cation environments of a given Fe^{3+} which contribute directly to QS and/or distort the oxygen octahedra in a different way. At 78 K, for samples with the wolframite structure, no measurable contribution of Fe^{2+} to the spectrum could be detected, but the Fe^{3+} peaks were considerably broadened relative to those at 294 K. However, for samples with the α-PbO_2 structure, an additional small broad peak is visible at larger positive velocities and undoubtedly arises from Fe^{2+}. In fact, a continuous weak absorption is noted in the positive velocity range up to $\approx +2.5$ mm/s relative to the baseline. The Fe^{3+} contribution could be adequately described by one doublet. Although a fit of the Fe^{2+} doublet is possible only with reduced accuracy, the isomer shift (IS) is typical for Fe^{2+}. For 294 K spectra, this contribution is evidently contained in the "Fe^{3+}" peaks. Hence, either there is a large T dependence of QS(Fe^{2+}) or a mixture of Fe^{2+} and Fe^{3+} is present due to electron exchange $Fe^{2+} \rightarrow Fe^{3+}$ with hopping times $< \approx 10^{-8}$ s (possibly related to electrical conduction), resulting in subspectra with IS intermediate between those of Fe^{2+} and Fe^{3+} (21–23). From area ratios of peaks, the relative concentration of Fe^{2+}, $[Fe^{2+}]/[\sum Fe]$, was approximately determined as $[Fe^{2+}]/[\sum Fe] \approx 0.07$. Samples prepared in a $N_2/O_2 = 30$ gas mixture exhibited an enhanced impurity phase as mentioned; for this reason, we did not use them for Mössbauer analysis.

2. $Fe_{1-x/3}Nb_{1+x/3}O_4$, $x = 0.02$ and 0.05

For $x = 0.02$, the spectra recorded did not differ appreciably from those for $x = 0$. The 294 K spectrum of $x = 0.05$ in the wolframite structure (preparation in air) shows also a weakly resolved doublet with broad lines (Fig. 2). The 79 K pattern reveals a minute additional broad peak at $\approx +2$ mm/s, which is undoubtedly due to Fe^{2+}. For the 294 K pattern, such a peak is absent as in the case of $x = 0$. At 79 K, the line width of the Fe^{3+} doublet is notably increased relative to that of the 294 K pattern, as for $x = 0$. The Mössbauer parameters for a two-doublet fit to the 79 K spectrum are given in Table 2. $[Fe^{2+}]/[\sum Fe] \approx 0.04$ was found; for full stoichiometry, 0.035 is expected using the previously mentioned chemical formula for the series. For the α-PbO_2 phase (preparation in air), a one-doublet fit at 294 K and a two-doublet fit at 79 K give comparatively large χ^2 in both cases. A one-doublet fit to the 294 K pattern was better than for $x = 0$. IS and QS can evidently be determined quite accurately although there are differences between the data points and the fitted curve in the negative velocity range. Also, a reasonable estimation of $[Fe^{2+}]/[\sum Fe] \approx 0.08$ is possible for the 79 K pattern. When the α-PbO_2 phase was obtained after heating in an atmosphere

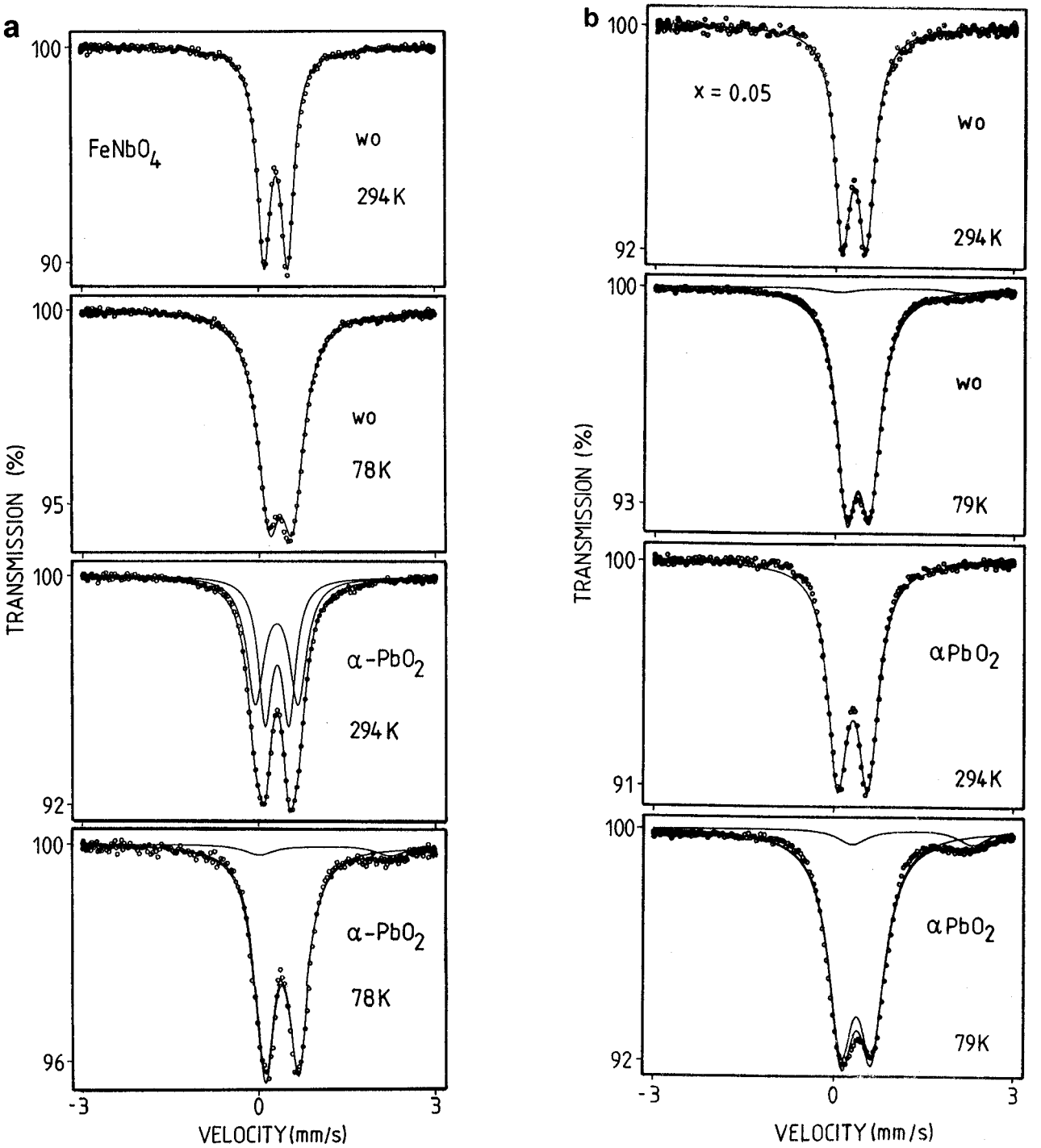

FIG. 2. ^{57}Fe Mössbauer spectra for annealed (wolframite structure (wo)) and quenched (α-PbO_2 structure) samples: (a) $FeNbO_4$ ($x = 0$); (b) $Fe_{1-x/3}Nb_{1+x/3}O_4$, $x = 0.05$.

with a $N_2/O_2 = 30$ gas mixture (exsolved secondary phases $< 0.1\%$ as estimated from light microscopic analysis), the same fits could be made. The Mössbauer parameters were very similar and from the 79 K spectrum $[Fe^{2+}]/[\sum Fe] \approx 0.11$ was derived; this means that $[Fe^{2+}]$ has increased. Such a situation could be associated with oxygen deficiency due to a too reducing atmosphere.

TABLE 2

^{57}Fe Mössbauer Parameters for Compositions $Fe_{1-x/3}Nb_{1+x/3}O_4$, $x = 0, 0.05$ (IS = Isomer Shift (Referred to Metallic Iron), QS = Quadrupole Splitting, B = Line Width)

Composition x	T (K)	Structure	IS(mm/s)		
			Fe^{2+}	Fe^{3+}	Fe^{3+}
0	294	wo		0.39	
	294	α-PbO_2		0.41	0.40
	79	wo		0.47	
	79	α-PbO_2	1.18	0.49	
0.05	294	wo		0.40	
	294	α-PbO_2		0.42	
	79	wo	1.32	0.39	
	79	α-PbO_2	1.39	0.39	

QS (mm/s)			B (mm/s)		
Fe^{2+}	Fe^{3+}	Fe^{3+}	Fe^{2+}	Fe^{3+}	Fe^{3+}
	0.39			0.24	
	0.40	0.72	0.70	0.28	
	0.40		0.46		
2.29	0.56		1.28	0.40	
	0.41			0.33	
	0.51			0.41	
2.10	0.39		0.69	0.41	
2.01	0.52		0.63	0.51	

ELECTRICAL RESULTS

1. Impedance Measurements

1.1. $FeNbO_4$ ($x = 0$)

Typical examples of plots of the real part of the impedance, Z', versus the imaginary part, Z'', in the complex impedance plane are illustrated in Fig. 3. From Fig. 3a, two semicircular arcs are seen at 98 K for the wolframite phase of $FeNbO_4$. Arc I is due to crystallites, and arc II can arise in principle from grain boundaries and/or interfacial electrode processes. The assignment is made on the basis of capacity data, derived from the relation $\omega_{max}\rho_{DC}^{AC}C = 1$ ($\omega = 2\pi\nu$, with ν = frequency), where $\omega_{max} = \omega$ at the maximum of a semicircle, ρ_{DC}^{AC} = DC resistivity extrapolated from Z' for $\omega \to 0$, and C = capacity (15). Arc I, with C in the low pF/cm range for ρ_{DC}^{AC}, evidently reflects the crystallite behavior; arc II, with larger C, is associated with other processes. In fact, we determined ρ_{DC}^{AC} of the interesting arc I by extrapolating $\omega \to \infty$ from arc II. In Fig. 3a, arc I is in fact a depressed circular arc, implying the center of the semicircle to be located below the Z' axis. Such a result is interpreted as a distribution $\Delta\tau$ of relaxation times $\tau = RC$ for a parallel circuit around an average value $\langle\tau\rangle$ instead of a discrete τ and the depression angle is related to τ (15). From data for samples cut to half of their original lengths, it follows that arcs I and II are reduced to half of their original sizes; hence, arcs II are due to grain boundary processes, while interfacial electrode processes obviously take place at frequencies < 20 Hz. The assignment of arcs is supported by data of voltage dependence. For arc I there was no measurable difference when the voltage applied to the sample electrodes was 1 V or 20 mV (RMS), in contrast to arcs II, which showed an increase up to a factor of 4–8 for ρ_{DC}^{AC} when the voltage was reduced from 1 V to 20 mV. The applied frequency window was too narrow at higher T and no reliable extrapolations could be carried out above ≈ 350 K. Fig. 3b demonstrates the analogous data of $FeNbO_4$ in the α-PbO_2 phase. Here, it appears that arc I is a more ideal semicircle than that for the wolframite phase. No marked differences to the above pictures are observed for $Fe_{1-x/3}Nb_{1+x/3}O_4$, $x = 0.02$ and 0.05.

The resistivity ρ_{DC}^{AC} is presented in Fig. 4 in the form $\log\rho_{DC}^{AC}$–$1/T$ in the low-T region. For each graph it is seen that the grain boundaries have larger resistivities than crystallites (current density $j < 1$ mA/cm^2). Above ≈ 350 K, four-terminal DC resistivity measurements were conducted (ρ_{DC}), as mentioned. Voltage-dependent DC measurements (10 mV to 4 V, sample dimensions $\sim 7 \times 1 \times 1.5$ mm^3) show that there is a marked effect up to higher T, as visible from Fig. 4a. The variation is not a heating effect of samples leading to an increase in T. For the highest applied DC voltage of 4 V, it appears that the ρ_{DC}–$1/T$ curve is parallel to ρ_{DC}^{AC}–$1/T$ for crystallites with about the same activation energy. Above ≈ 600 K, the voltage dependence of ρ_{DC} becomes rather low. It is evident from Fig. 4 that a simple law $\rho = \rho_0 \exp(E_A/kT)$($E_A$ = activation energy) with a fixed E_A does not describe the conduction mechanism in a larger T range. The bending of our $\log\rho_{DC}^{AC}$–$1/T$ curve is less marked than that presented in ref. 9. For the α-PbO_2 structure, analogous curves were observed (Fig. 4b); $\rho_{DC}^{AC}(100\,\text{K}) \sim 4 \times 10^4\,\Omega$cm is ca. a factor of 10 less than $\rho_{DC}^{AC}(100\,\text{K})$ for the wolframite structure.

Activation energies E_A deduced in the high- and low-T regions are quoted in Table 3. For hopping processes of small polarons such a variation is expected from theory when optical phonons are dominating at high T and acoustic phonons at low T (24). The very similar shape of the resistivity curves in Fig. 4 for crystallites and grain boundaries suggests that the conduction mechanisms are basically the same. The rather semicircle-like shape of Z' versus Z'' for grain boundaries (Fig. 3) implies also here largely a simple parallel equivalent circuit to be acting (15). For an interpretation of the strong voltage dependence of this process at low T, a more detailed examination is necessary. We found that the varying gas atmospheres (O_2, air, $N_2/O_2 = 30$) applied during the preparation of $FeNbO_4$ have a strong effect on the grain boundary resistivity; the latter seems to be largest for O_2 treatment. For the resistivity, there appears to be a difference between the wolframite and α-PbO_2

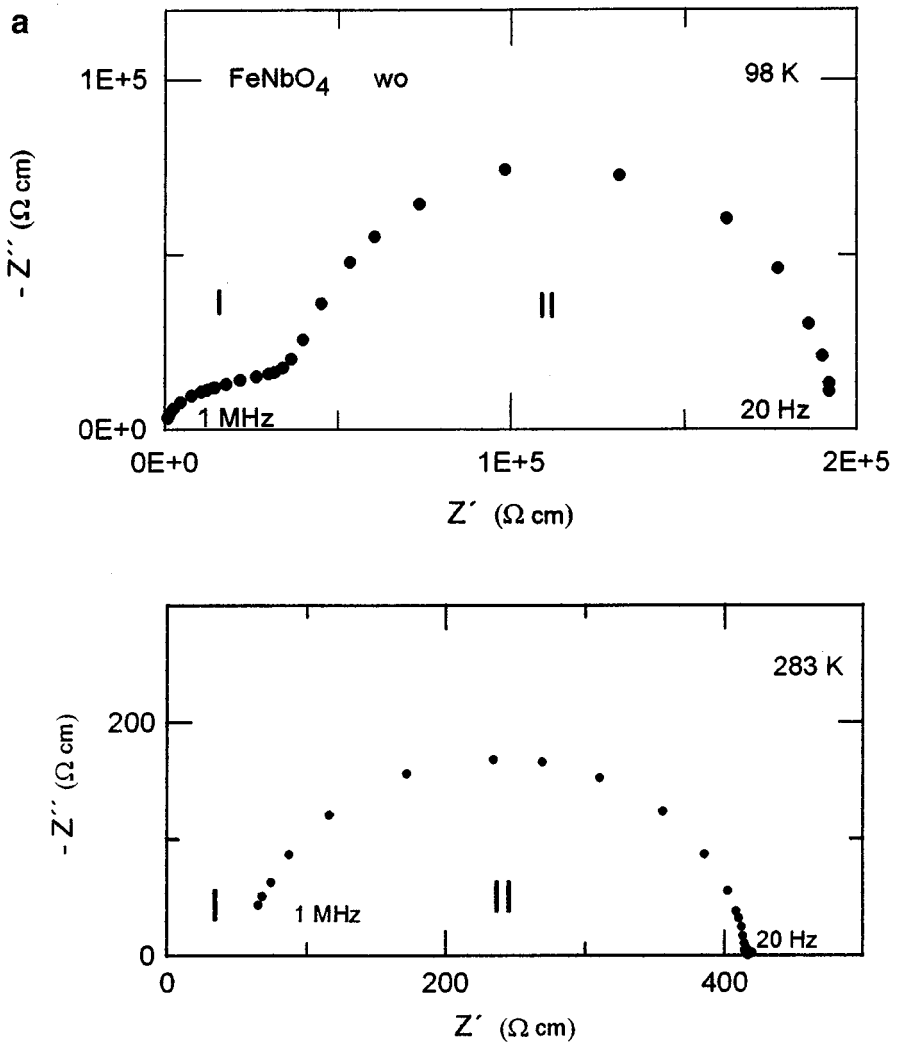

FIG. 3. Complex plane impedance plots of the real part Z' versus the imaginary part Z'' for $FeNbO_4$, showing different types of semicircular arcs: (a) wo structure; (b) α-PbO_2 structure.

phases since in the latter case, at the highest T, an activation energy $E_A \approx 0.70$ eV is observed which may arise from intrinsic conduction, whereas this process seems to be absent in the wolframite phase in the same T range where $E_A \approx 0.3$ eV was deduced; also in the lower T ranges, E_A is smaller in the wolframite structure (Fig. 4a, b).

In the low-T region, we tried to check a possible $\ln \rho_{DC}^{AC} \propto -(T_0/T)^{1/4}$ law after Mott that describes the variable range hopping (VRH) mechanism (25) (Fig. 5). It appears that such a relation may hold in the low-T range, although this check has to be extended to still lower T. The VRH tunneling charge transport has been found to occur at $T < \sim 10$ K in compensated semiconductors from shallow occupied to unoccupied donor states that exhibit a spread of energies. On the other hand, for our samples the VRH law appears to extend to far higher T. Such a case has also been observed in other disordered semiconductors (26, 27). Theoretically, the occurrence of the foregoing relationship up to higher T has been predicted for deep hopping states in the case of acoustic-phonon-assisted hop processes using different approaches (28–30). However, for disordered semiconductors with localized states close to the Fermi level and electron–electron Coulomb interactions, a dependence of the type $-(T_0/T)^{1/2}$ has also been derived (31).

1.2. $Fe_{1-x/3}Nb_{1+x/3}O_4$, $x = 0.02$ and 0.05

For $x = 0.05$ it becomes obvious from Fig. 4c that in the wolframite structure for crystallites $\rho_{DC}^{AC}(100\,K) \approx 2 \times 10^4\,\Omega$cm is ca. a factor of 10 lower than $\rho_{DC}^{AC}(100\,K) \approx 2.5 \times 10^5\,\Omega$cm for $FeNbO_4$, whereas for the α-PbO_2 structures $\rho_{DC}^{AC}(100\,K) \approx 3 \times 10^5\,\Omega$cm in contrast to $\rho_{DC}^{AC}(100\,K)$

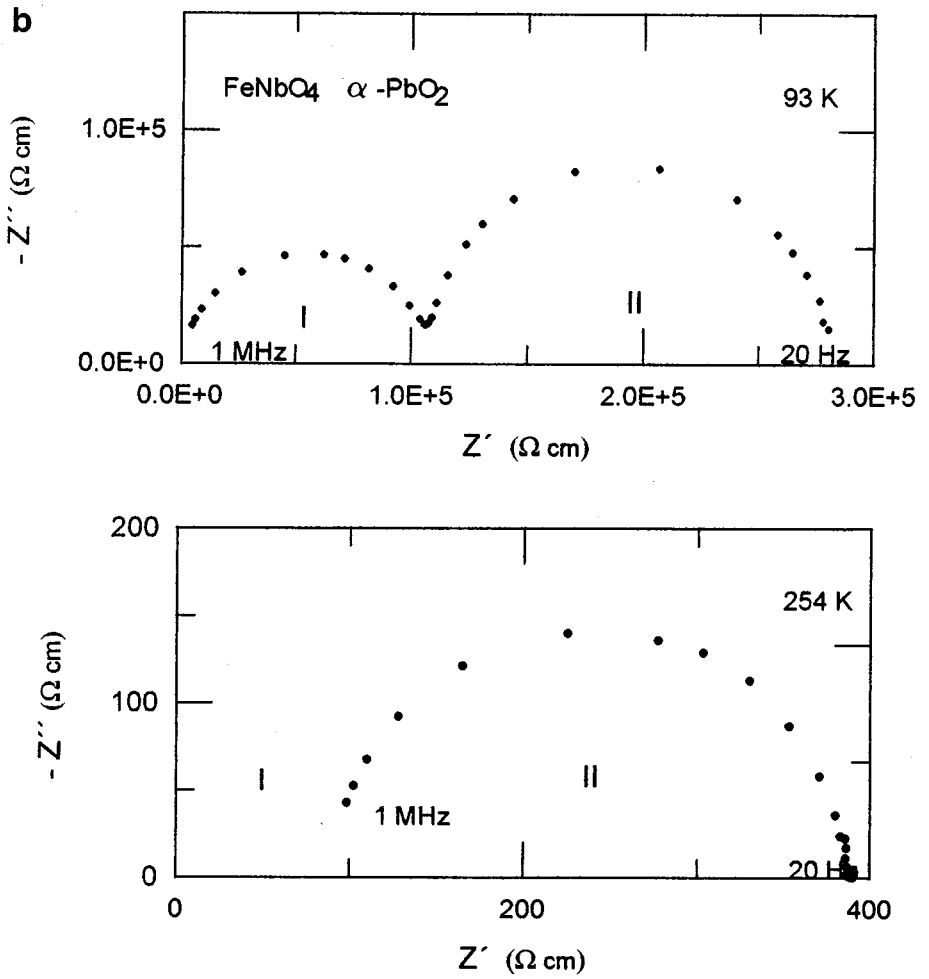

FIG. 3—*Continued*

$\approx 4 \times 10^4\,\Omega$cm for $FeNbO_4$; the data for $x = 0.02$ are in between these results. Very similar relations for $x = 0$ and 0.05 also hold at 294 K. In the high-T range, activation energies $E_A = 0.16$ and 0.25 eV for the wolframite and α-PbO_2 phases of $x = 0.05$, respectively, are inferred, whereas 0.30 and 0.74 eV, respectively, are found for $FeNbO_4$ (Table 3). The high value 0.74 eV points to a different conduction process, as mentioned.

In the low-T region, a plot of $\ln \rho_{DC}^{AC}$ versus $T^{-1/4}$ in the wolframite structure also gives an approximate straight line as for $FeNbO_4$ (Fig. 5).

2. Thermopower

2.1. *$FeNbO_4$ ($x = 0$)*

The thermopower Θ is negative at all T, whence n-type conduction follows and the majority of charge carriers are electrons. Experimental data are reproduced as a Θ versus T plot in Fig. 6. In the low-T region, a slightly bent curve is noted with increasing $|\Theta|$ for rising T for both crystal structures; at higher T, the rise in $|\Theta|$ slows down and $|\Theta|$ becomes constant. We did not extend the measurements to $T > \approx 900$ K because of a possible transition of the α-PbO_2 to the wolframite structure. Both graphs were reproducible to $\pm 5\,\mu$V/K; all data were taken after the first run to higher T.

$T \leq 300$ K. At low T, the experimental data of samples with the wolframite structure can be adequately described by a $\Theta = AT^{1/2} + B$ law between ≈ 120 and 300 K rather than by a linear relation $\Theta = AT + B$ that applies possibly to the results for samples with the α-PbO_2 structure; however, to decide this point definitely, very accurate Θ data are necessary. The former law is predicted in the case of a VRH mechanism, where it is theoretically $\Theta = AT^{1/2}$ when the density of localized states is slowly varying (32); an additional T-independent constant B is expected in the case of electron correlations. On the other hand, a linear Θ–T relation is derived for small polaron hopping among inequivalent sites with a broad energy variation (33). A very

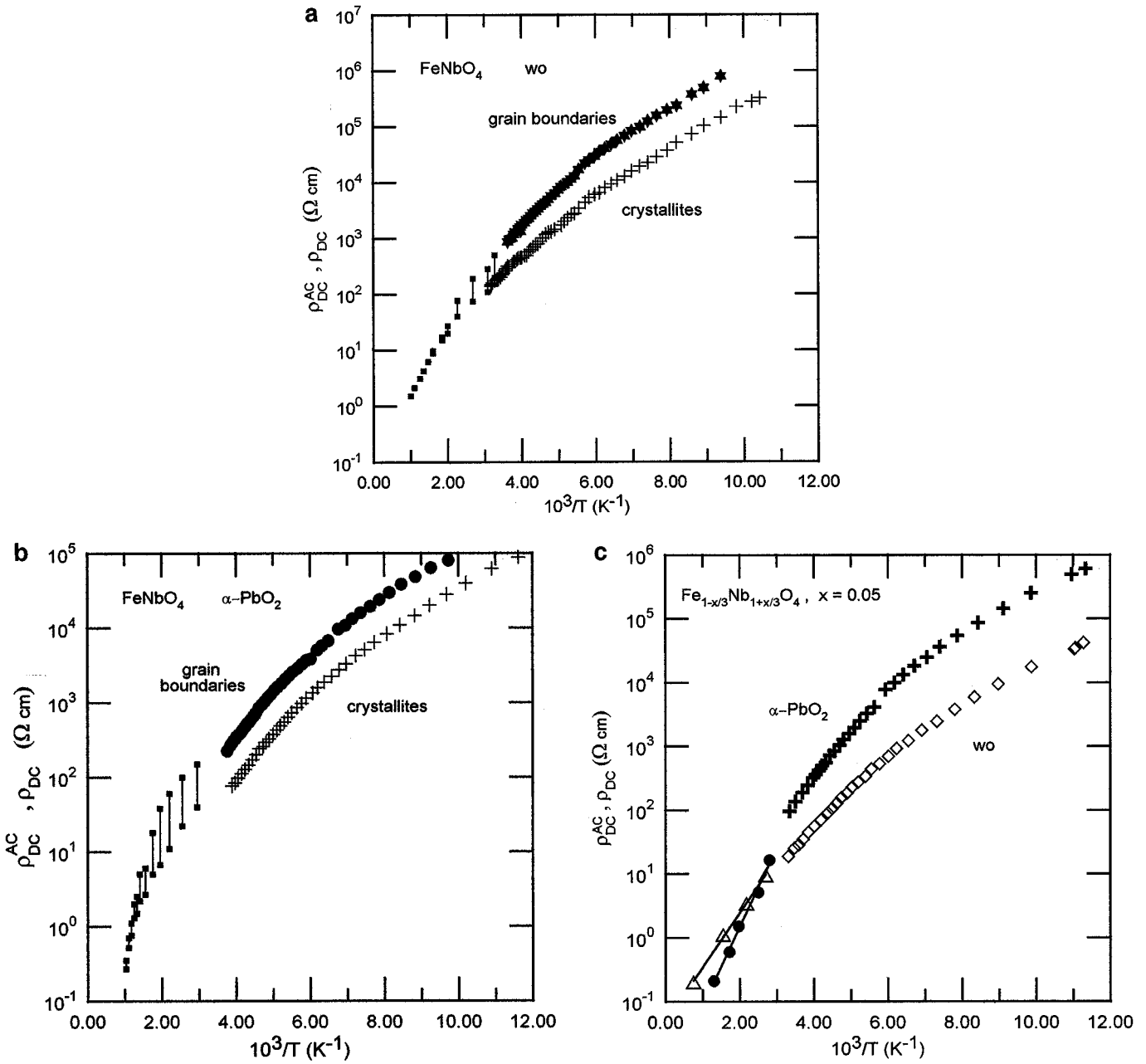

FIG. 4. Variation of $\log \rho_{DC}^{AC}$ (data determined by impedance spectroscopy, current density $j < 1\,mA/cm^2$) and of $\log \rho_{DC}$ with $1/T$; DC resistivity ρ_{DC} results are presented as bars indicating the current density dependence of ρ_{DC} due probably to grain boundary effects. Upper ends of bars correspond to $j \approx 1\,mA/cm^2$, lower ends to $j \approx 100\,mA/cm^2$. (a) ρ_{DC}^{AC}: (+) crystallites, (★) grain boundaries. (b) ρ_{DC}^{AC}: (+) crystallites, (●) grain boundaries. (c) ρ_{DC}^{AC} (low T): (□) crystallites (wo), (+) crystallites (α-PbO_2); ρ_{DC} (40 mA/cm^2) (high T): (△) crystallites (wo), (●) crystallites (α-PbO_2).

similar behavior for σ and Θ as for $FeNbO_4$ at low T has been noted for some compositions of $Cr_{1-x}Nb_xWO_4$ solid solutions (34). Furthermore, for boron carbide $B_{1-x}C_x$ a linear Θ–T relationship has been observed (33, 35).

Assuming an $Fe^{2+} \rightarrow Fe^{3+}$ small polaron hopping process as the dominating conduction mechanism, we suggest either a Θ rather invariable with T or a linear Θ–$1/T$ relation in a larger T range, as has been noted for spinels (19, 36–39). From $\Theta = k/e(E_\Theta/T + \alpha)$ (k = Boltzmann constant, e = electronic charge, E_Θ = activation energy for Θ, α = constant), it is expected that $E_\Theta < E_A$ for a hopping charge transport (E_A = activation energy for electrical

TABLE 3
Activation Energies E_A Inferred from Resistivity Data of Fig. 4[a]

Composition x	E_A (eV)			
	Low T		High T	
	wo	α-PbO_2	wo	α-PbO_2
0	0.045	0.05	0.3	0.74
0.05	0.05	0.06	0.16	0.25

[a] At low temperatures, E_A is taken from ρ_{DC}^{AC}, at high temperatures from ρ_{DC}; wo = wolframite structure, α-PbO_2 = α-PbO_2 structure.

conduction) (40). In transition metal oxides (polar crystals) we have to face the effect of a strong polarization of the lattice around a hopping electron, giving an enhanced E_A of the resulting polaron (25). In our case, a possible inequivalence of hopping sites in the wolframite structure could in part be associated with nonstoichiometry, giving rise to lattice defects for too low or high oxygen partial pressures during sample preparation. A further effect of disorder may be an incomplete ordering of the FeO_6 and NbO_6 chains. In the α-PbO_2 structure, predominant disorder is generated by the random distribution of Fe and Nb cations, probably enhanced by an eventual nonstoichiometry.

$T \geq 300$ K. Θ for hopping charge conduction in the case $kT \gg \Delta$ or J (Δ = spread of localized energy levels, J = small polaron band width) is given by

$$\Theta = (k/e)\,[\ln n/\beta(N-n) + \alpha], \qquad [1]$$

where N = concentration of sites available for hopping charge carriers, n = concentration of carriers, β = spin-degeneracy factor, which is assumed to take on values of 1 or 2, and αkT = kinetic energy of charge carriers, which is assumed to be low (25, 40). We derive in the high-T limit for samples with the wolframite structure an experimental $\Theta \sim -270\,\mu V/K$ and for those with the α-PbO_2 structure $\Theta \sim -230\,\mu V/K$. The plateau of Θ in the high-T limit for spinel ferrites, where $Fe^{2+} \rightarrow Fe^{3+}$ hopping is assumed to be the prevailing conduction mechanism, has been applied to determine cation distributions using the Heikes formula, i.e., Eq. [1] setting $\alpha = 0$ and applying $\beta = 2$ (41, 42). Θ for polycrystalline samples is, in general, assumed to be representive for crystallites; however, a grain boundary effect, as observed for our resistivity data, cannot be excluded. In the literature, little information can be found as to differences in Θ for poly- and monocrystalline semiconducting metal oxides with the exception of spinel ferrites, where a small effect was established (18, 43, 44); the same was found for compositions $Cr_{1-x}W_{1+x}O_4$ (45).

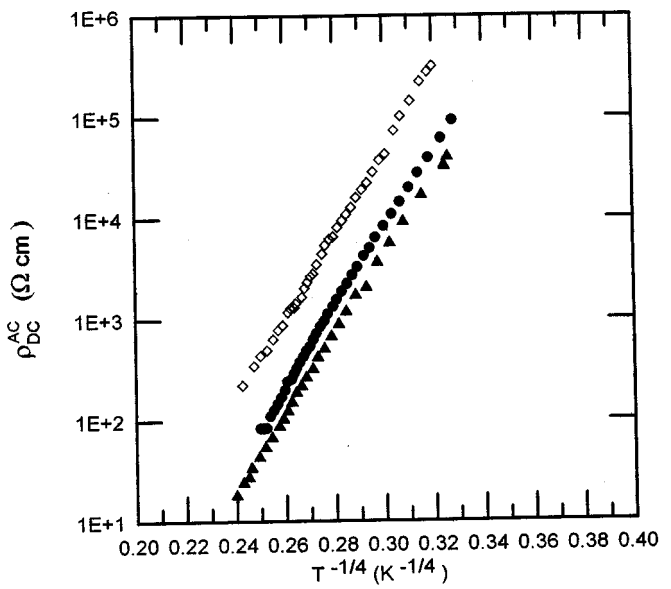

FIG. 5. $\ln \rho_{DC}^{AC} \propto T^{-1/4}$ plots for $FeNbO_4$ [(●) wo, (□) α-PbO_2] and $Fe_{1-x/3}\,Nb_{1+x/3}O_4$, $x = 0.05$ [(▲) wo].

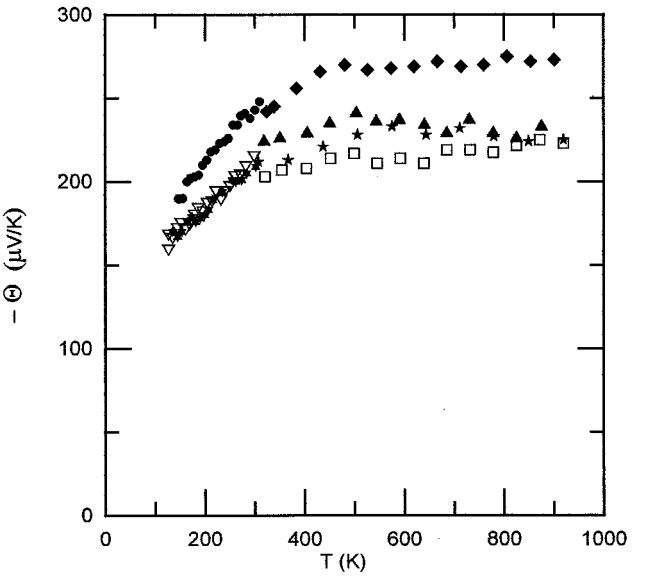

FIG. 6. Temperature variation of the thermopower Θ: (●, ◆) $FeNbO_4$ (wo); (▲, ▽) $FeNbO_4$ (α-PbO_2); (★) $x = 0.05$ (wo); (□) $x = 0.05$ (α-PbO_2).

2.2. $Fe_{1-x/3}Nb_{1+x/3}O_4$, $x = 0.02$ and 0.05

Θ data for $x = 0.05$ are illustrated in Fig. 6; results for $x = 0.02$ are not typically different from those of $x = 0$; therefore they are not presented. There appears also to

occur a linear Θ–$T^{1/2}$ or Θ–T relationship at $T \approx < 300\,\mathrm{K}$ as for samples with $x = 0$. The slope and the magnitude of Θ are in fact identical to Θ of $x = 0$ with the α-PbO_2 structure. In the high-T region, Θ becomes constant with $\Theta \sim -225\,\mu\mathrm{V/K}$ for both structures.

For $x = 0.02$ and 0.05, a larger Fe^{2+} population is expected than for $FeNbO_4$ since these compositions are members of a mixed crystal series, as mentioned, which is described by $Fe_{1-x/3}Nb_{1+x/3}O_4$ or, discriminating between Fe^{2+} and Fe^{3+}, by $Fe^{2+}_{2x/3}Fe^{3+}_{1-x}Nb^{5+}_{1+x/3}O_4$. Theoretically, for $x = 0.02$ and 0.05 it should be $[Fe^{2+}]/[Fe^{3+}] = 0.0136$ and 0.0350, respectively, whereas no $[Fe^{2+}]$ is expected in stoichiometric $x = 0$. To analyze the increase in $[Fe^{2+}]$, starting from $x = 0$, we concentrated on $x = 0.05$ since $[Fe^{2+}]$ should show a more marked effect on ρ and Θ than for $x = 0.02$, provided charge transfer occurs by electron hopping between Fe^{2+} and Fe^{3+}. In this context we have to face a possible reduction of a low concentration of Nb^{5+} to Nb^{4+} in the presence of Fe^{2+} and Fe^{3+}. In such a case, there may also occur electron jumps between Nb^{4+} and Nb^{5+}, most probably with an activation energy differing from that for jumps between Fe cations. The presence of Nb^{4+} may go hand in hand with a too low $[Fe^{2+}]$. Such a situation can be thought of also for completely stoichiometric compositions. If cation or oxygen deficiency or excess occurs, $[Fe^{2+}]$ and $[Nb^{4+}]$ can in principle be different.

DISCUSSION

1. Mössbauer Spectra

From the Mössbauer data of $x = 0$, 0.02, and 0.05, it becomes evident that the local Fe^{3+} environments in the wolframite and α-PbO_2 structures show a notable difference. This is concluded from the quadrupole splitting (QS) and line width (B) of Fe^{3+} doublets for both structures (Table 2). The effect may be related to conductivity when charge transport occurs via electron hopping between Fe^{2+} and Fe^{3+} as suggested (1). In this case, the 294 K spectra can provide information (Fig. 2) if the continuous weak absorption in the positive velocity range can be interpreted as being due to electron hopping processes as could be shown for very similar spectra of spinels (21). The Fe^{2+} contribution to the spectra, although doubtless present, is too low for a detailed examination. From Fig. 2 it can be clearly seen that one Fe^{2+} doublet cannot adequately describe the Fe^{2+} pattern. A second Fe^{2+}-like subspectrum may improve the fit; however, due to the low intensity, the error would be high.

2. Resistivity

The main goal of this work is directed toward electrical conduction in crystallites for the wolframite and α-PbO_2 phases. If $Fe^{2+} \rightarrow Fe^{3+}$ electron hopping gives rise to the relatively low resistivity ρ, one may suggest a difference in ρ for both structures. In the ordered state, zigzag chains of FeO_6 octahedra along [001] may favor electron motion of the above type across common edges of FeO_6 octahedra (Fe–Fe ≈ 0.31 nm) or by a transport via Fe^{2+}–O–Fe^{3+} (Fig. 1). This kind of charge transport would evidently be interrupted by NbO_6 octahedra in the chain for a not perfectly ordered crystal. Such a situation may also take place in the wolframite samples for $FeNbO_4$, since a tiny amount of a secondary phase ($< 0.5\%$, suggestedly α-Fe_2O_3 (1)) was detected by light microscopy, which may result in a very weak surplus of Nb^{5+}. Nothing appears to be known of a possible incorporation of cation or oxygen vacancies in the crystals. The enhanced concentration of Fe^{2+} in $FeNbO_4$ with the α-PbO_2 structure, as found from Mössbauer data, must be compensated for by a process balancing positive and negative charges. This phenomenon may be connected to oxygen vacancies. We do not believe that the tiny amount of segregated secondary phase in $FeNbO_4$ can be responsible for the large Fe^{2+} concentration. A more detailed analysis of charge carrier transport is based on Θ data, which are discussed in the following section.

For compositions $x = 0.02$ and 0.05, the Nb^{5+} concentration in FeO_6 chains is progressively enhanced with rising x for the wolframite structures, whereas for both compositions a random distribution of Fe and Nb exists in the α-PbO_2 phase. From Fig. 4 a difference in ρ^{AC}_{DC} is restricted to a factor of ~ 10 in all cases. Interpreting the data in terms of one kind of charge carrier, $\sigma = en\mu_D$ is valid (n = charge carrier density, μ_D = drift mobility), where for a hopping charge transport n is fixed, μ_D is determined by phonon-assisted hops, and σ can vary by orders of magnitude. In the case of an $Fe^{2+} \rightarrow Fe^{3+}$ polaron hopping process, we tentatively assume $n \sim 10^{21} Fe^{2+}/cm^3$ (which is compatible with the experimental data) whence it follows from the experimental $\rho^{AC}_{DC}(300\,\mathrm{K})$ that $\mu_D(300\,\mathrm{K}) \approx 1 \times 10^{-4}\,(\mathrm{cm^2/V\,s})$. Such a value is typical for low-mobility polar semiconductors in which a small polaron hopping charge transport occurs (40).

Applying in the low-T region a law $\ln \sigma^{AC}_{DC} \propto A(T_0/T)^{1/4} + B$ for the extrapolated data (Fig. 5), we infer for all samples values of T_0 of the order $T_0 \sim 4 \times 10^7\,\mathrm{K}$. Such a magnitude is indeed assumed to occur by theory for T far above that for liquid helium (29). In the high-T region, we adopt adiabatic or nonadiabatic small polaron hopping transport for the wolframite phase of $FeNbO_4$; the experimental $E_A = 0.2$–$0.3\,\mathrm{eV}$ is compatible with literature values for transition metal compounds where charge transport is attributed to small polaron conduction. However, the large $E_A = 0.7\,\mathrm{eV}$ for the α-PbO_2 phase points to a different conduction mechanism, possibly to intrinsic conduction. For composition $x = 0.05$, such a situation appears to be absent because of lower E_A values.

3. Thermopower

$T \leq 300$ K. In many transition metal oxides with hopping charge conduction, Θ was found to give a straight line on a Θ–$1/T$ plot at not too high T, as mentioned; an activation energy E_Θ can be derived that is lower than that inferred from conductivity data and this is characteristic for a hopping charge transport (39). On the other hand, for small polaron hopping of the type $Fe^{2+} \rightarrow Fe^{3+}$, the available literature does not show unambiguous results; this can possibly be associated in part with nonstoichiometry of the related oxides, which may exert a large influence on the charge transport. In contrast, in the high-T limit, when Θ becomes constant and the Heikes formula applies, data for spinel ferrites are available (37, 38, 41–44, 46). In our case, a series of measurement runs for $x = 0$ in the wolframite structure resulted in data that are more consistent with straight lines on Θ–$T^{1/2}$ than Θ–$1/T$ plots for $T < 300$ K. Linear Θ–T curves describe possibly better results for $x = 0$ in the α-PbO_2 structure and for $x = 0.05$ in both structures (Fig. 6).

For the analyzed oxides it is tentatively assumed that there is a low-lying full O $2p$ band and empty conduction bands of probably Fe $4s$ and Nb $5s$ states with an intermediate narrow Fe^{3+} $3d$ and an empty Nb^{5+} $5d$ band; both bands may be divided into subbands with spin up and spin down. Localized Fe^{2+} may act as predominant donors; furthermore, impurity donor or acceptor states can be expected, probably effected by oxygen nonstoichiometry. In addition, one has to take into account a probable Me–O hybridization (Me = metal cation). At present, it would be highly speculative to give exact positions of the levels in the energy band gap. A model that describes the energy scheme in detail has to consider additional effects: (1) cation order and disorder and additional disorder by nonstoichiometry can be associated with a mobility edge (25); (2) possible electron–electron interactions may lead to a Coulomb gap, resulting in a strong reduction of the density of states.

$T \geq 300$ K. Applying tentatively the $Fe^{2+} \rightarrow Fe^{3+}$ election hopping process model and utilizing Eq. [1], with $N = [Fe^{3+}] + [Fe^{2+}]$, $n = [Fe^{2+}]$, $\alpha = 0$, and $\Theta = -270\,\mu V/K$ for the wolframite structure, the ratio $n/(N-n) = [Fe^{2+}]/[Fe^{3+}] \approx 0.044$ with $\beta = 1$; however, no ratio could be determined from Mössbauer spectroscopy. The value $\beta = 1$ should be adequate in a magnetically ordered state or in the presence of a very high magnetic field; for $\beta = 2$, the $[Fe^{2+}]/[Fe^{3+}]$ ratio is twice as high. For the α-PbO_2 lattice, with $\Theta = -230\,\mu V/K$ and $\beta = 1$, the ratio $[Fe^{2+}]/[Fe^{3+}] = 0.069$, whereas ~ 0.078 is obtained from the Mössbauer spectrum, in close agreement. Recently, a generalization of the Heikes formula has been proposed for charge hopping effected by mixed-valence cations Me^{n+} and $Me^{(n+1)+}$ (Me = cation) (47), based on the model of ref. 48, with $\beta = (2S_n + 1)/(2S_{n+1} + 1)$, where S_n and S_{n+1} = cation spins. In our case, where $S(Fe^{2+}) = 2$ and $S(Fe^{3+}) = \frac{5}{2}$, $\beta = \frac{5}{6}$; this is very close to $\beta = 1$, which is consistent with our experimental Θ and Mössbauer data. From this crude estimate, we conclude that $Fe^{2+} \rightarrow Fe^{3+}$ hopping charge transport, where all Fe^{2+} and Fe^{3+} take part in conduction, seems to be compatible with all experimental data for the α-PbO_2 structure, but the participation of only part of all available Fe cations in conduction cannot be excluded.

For $x = 0.05$, the number for the wolframite structure with $\Theta \sim -225\,\mu V/K$ and with $\beta = 1$ is $[Fe^{2+}]/[Fe^{3+}] = 0.078$ whereas the Mössbauer data give ~ 0.04; for the α-PbO_2 structure with the same Θ, the Mössbauer results give ~ 0.08, in good agreement.

In the present situation, one may speculate as to the microscopic processes of charge transport. The suggestion of a transport of the kind $Fe^{2+} \rightarrow Fe^{3+}$ should give lower resistivities with increasing $[Fe^{2+}]$. A tempting mechanism may be preferred charge transport along [001] in the wolframite structure. However, due to the random distribution of crystallites, no conclusions are possible with regard to anisotropic behavior. In both phases, on the other hand, the presence of Fe^{2+} may favor configurations such as Fe^{2+}–Nb^{5+} for microscopic charge balance reasons. In this case, the activation energy for the release of an electron from Fe^{2+} may be higher. One probably has to distinguish between different kinds of Fe^{2+} as charge transport is concerned, and theoretically only part of all Fe^{2+} may take part in long-range charge transport; on the other hand, from the foregoing estimates a participation of all Fe in charge transport seems to be compatible with the experimental data.

CONCLUSION

The DC conductivity σ_{DC}, the extrapolated crystallite conductivity σ_{DC}^{AC}, and the thermopower Θ data for compositions $Fe_{1-x/3}NB_{1+x/3}O_4$ with $x = 0, 0.02$, and 0.05 in the wolframite and α-PbO_2 structures show features typical for small polaron hopping charge transport at high and low temperatures T.

From the validity of a variable-range hopping law $\ln \sigma_{DC}^{AC} \propto -(T_0/T)^{1/4}$ up to temperatures well above ~ 100 K, it follows that a theoretical model may apply, developed for electron hopping between deep localized states; this interpretation is also consistent with the experimental Θ data. Assuming electron hopping of the type $Fe^{2+} \rightarrow Fe^{3+}$, the concentration ratio $[Fe^{2+}]/[Fe^{3+}]$ deduced from Θ data at high temperatures is in part in close agreement with that determined from ^{57}Fe Mössbauer spectra at 79 K. The result appears to indicate that in this case all Fe^{2+} and Fe^{3+} are taking part in conduction, at least at higher temperatures. It seems as if cation disorder in the suggested ordered wolframite phase of $FeNbO_4$ plays an essential part in conduction, evidently resulting in hopping

charge transport. Whether lattice defects are notably involved in the hopping transport is not quite clear.

ACKNOWLEDGMENT

This work was supported by a grant from the Deutsche Forschungsgemeinschaft.

REFERENCES

1. J. Koenitzer, B. Khazai, J. Hormadaly, R. Kershaw, K. Dwight, and A. Wold, *J. Solid State Chem.* **35,** 128 (1980).
2. H. Schröcke, *Neues Jahrb. Mineral. Abh.* **106,** 1 (1966).
3. H. Weitzel and H. Schröcke, *Neues Jahrb. Mineral. Abh.* **119,** 285 (1973).
4. A. C. Turnock, *J. Am. Ceram. Soc.* **49,** 177 (1966).
5. C. Keller, *Z. Anorg. Allg. Chem.* **318,** 89 (1962).
6. F. Laves, G. Bayer, and A. Panagos, *Schweiz. Mineral. Petrogr. Mitt.* **43,** 216 (1963).
7. R. S. Roth and J. L. Waring, *Am. Mineral.* **49,** 242 (1964).
8. H. Brunner and R. Gruehn, *Z. Naturforsch., B* **31,** 318 (1976).
9. Y. Noda, M. Shimada, M. Koizumi, and F. Kanamaru, *J. Solid State Chem.* **28,** 379 (1979).
10. M. Harder and H. K. Müller-Buschbaum, *Z. Anorg. Allg. Chem.* **456,** 99 (1979).
11. W. T. A. Harrison and A. K. Cheetham, *Mater. Res. Bull.* **24,** 523 (1989).
12. H.-F. Cheng, *J. Appl. Phys.* **56,** 1831 (1984).
13. J. T. S. Irvine, A. Huanosta, R. Valenzuela, and A. R. West, *J. Am. Ceram. Soc.* **73,** 729 (1990).
14. O. Parkash, H. S. Tewari, V. B. Tare, D. Kumar, and L. Pandey, *J. Am. Ceram. Soc.* **75,** 3141 (1992).
15. J. R. Macdonald, "Impedance Spectroscopy." Wiley, New York, 1987.
16. J. P. Moore and R. S. Graves, *J. Appl. Phys.* **44,** 1174 (1973).
17. A. V. Gold, D. K. C. MacDonald, W. B. Pearson, and I. M. Templeton, *Philos. Mag.* **5,** 765 (1960).
18. A. J. M. Kuipers and V. A. M. Brabers, *Phys. Rev.* **14,** 1401 (1976).
19. T. E. Whall, K. K. Yeung, and Y. G. Proykova, *Philos. Mag. B* **54,** 505 (1986).
20. B. A. Griffiths, D. Elwell, and R. Parker, *Philos. Mag.* **22,** 163 (1970).
21. F. K. Lotgering and A. M. Van Diepen, *J. Phys. Chem. Solids* **38,** 565 (1977).
22. G. Amthauer and G. R. Rossman, *Phys. Chem. Miner.* **11,** 37 (1984).
23. F. J. Litterst and G. Amthauer, *Phys. Chem. Miner.* **10,** 250 (1984).
24. J. Schnakenberg, *Phys. Status Solidi* **28,** 623 (1968).
25. I. G. Austin and N. F. Mott, *Adv. Phys.* **18,** 41 (1969).
26. A. Gosh, *Phys. Rev. B* **42,** 5665 (1990).
27. L. Zuppiroli and L. Forro, *Phys. Lett. A* **141,** 181 (1989).
28. V. Ambegaokar, B. I. Halperin, and J. S. Langer, *Phys. Rev. B* **4,** 2612 (1971).
29. D. Emin, *Phys. Rev. Lett.* **32,** 303 (1974).
30. G. P. Triberis and L. R. Friedman, *J. Phys. C: Solid State Phys.* **18,** 2281 (1985).
31. A. L. Efros and B. I. Shklovskii, *J. Phys. C: Solid State Phys.* **8,** L49 (1975).
32. I. P. Zvyagin, The hopping thermopower, *in* "Hopping Transport in Solids" (M. Pollak and B. Shklovskii, Eds.). Elsevier, Amsterdam, 1991.
33. C. Wood and D. Emin, *Phys. Rev.* **29,** 4582 (1984).
34. Y. J. Shin, J. P. Doumerc, P. Dordor, M. Pouchard, and P. Hagenmuller, *J. Phys. Chem. Solids* **54,** 25 (1993).
35. H. Werheit and K. D. Groot, *Phys. Status Solidi B* **97,** 229 (1980).
36. J. Philips, T. E. Whall, and V. A. M. Brabers, *Philos. Mag. B* **71,** 23 (1995).
37. V. A. M. Brabers, *Physica B* **205,** 143 (1995).
38. J. Töpfer, A. Feltz, P. Dordor, and J. P. Doumerc. *Mater. Res. Bull.* **29,** 225 (1994).
39. N. F. Mott and E. A. Davis, "Electronic Processes in Non-crystalline Materials." Clarendon Press, Oxford, 1979.
40. A. Bosman and H. Van Daal, *Adv. Phys.* **19,** 1 (1970).
41. C. C. Wu, S. Kumarakrishnan, and T. O. Mason, *J. Solid State Chem.* **37,** 144 (1981).
42. A. Trestman-Matts, S. E. Dorris, and T. O. Mason, *J. Am. Ceram. Soc.* **67,** 69 (1984).
43. D. C. Carter and T. O. Mason, *J. Am. Ceram. Soc.* **71,** 213 (1988).
44. D. S. Erickson and T. O. Mason, *J. Solid State Chem.* **59,** 42 (1985).
45. J. P. Doumerc, W. Yangshu, P. Dordor, E. Marquestaut, M. Pouchard, and P. Hagenmuller, *J. Phys. Chem. Solids* **51,** 467 (1990).
46. B. Gillot and M. Nohair, *Phys. Status Solidi* **148,** 239 (1995).
47. J.-P. Doumerc, *J. Solid State Chem.* **110,** 419 (1994).
48. P. M. Chaikin and G. Beni, *Phys. Rev. B* **13,** 647 (1976).